Carbon mobilised at shallow depths in subduction zones by carbonatitic liquids

Stefano Poli[1]

More than half a gigaton of CO_2 per year is recycled in the Earth interior at convergent margins[1]. At least 40% of this CO_2 returns to the atmosphere via igneous activity at subduction zones[2-4]. Experimental and thermodynamic modelling of phase relationships at high pressure indicate that decarbonation or carbonate dissolution in fluids account for only a portion of CO_2 released[5], and that carbonatitic melts from a subducting crust are feasible only if thermal relaxation occurs at sub-arc depth. Here I experimentally demonstrate that Ca-rich hydrous carbonatitic liquids can be generated at temperatures as low as 870-900 °C at 120 km depth. I find that H_2O strongly depresses the solidus for hydrous carbonated gabbro, and, prospectively, for impure limestones. The resulting Ca-rich carbonatitic liquids can efficiently scavenge volatiles, Ca and Si from the slab and represent a potentially significant pathway for slab decarbonation. Such liquids are expected to be extremely mobile and reactive in a percolated mantle wedge, where they generate carbonate pyroxenites, a fertile CO_2 source for magmatism at subduction zones. This process is most effective at warm convergent margins and could correlate with the high CO_2 content of undegassed magmas.

The CO_2 returned to the atmosphere at convergent margins is mostly supplied by magmas, which are able to contain percent level of CO_2 in undifferentiated melts[4], along with H_2O contents typically not larger than 6 – 7 wt%. Progressive decomposition of OH-bearing minerals with depth efficiently accounts for H_2O recycling in arcs; on the contrary, subsolidus decarbonation has been modelled as an inefficient process in transferring CO_2 from the slab to the mantle wedge[6]. Ternary, (Ca,Fe,Mg)–carbonates are very stable at high pressure[3,5-10]. A viable mechanism considered for

[1] Dipartimento di Scienze della Terra, Università degli Studi di Milano, Via Botticelli 23, 20133, Milano, Italy

CO_2 fractionation in a mobile phase is dissolution in aqueous fluids released by breakdown of hydrous phases, although the efficiency of this process has been tested at moderate pressures only (< 2 GPa) [11,12].

Carbonatitic melts, as media able to mobilize carbon out of the slab at shallow depth (< 5GPa), are commonly regarded to be restricted to unusually hot regimes because minimum temperatures found for carbonatitic liquids are in the order of 1020-1100°C at 3 – 5 GPa[8-10,13,14]. However, H_2O is known to cause a profound depression of the liquidus surface for $CaCO_3$; the temperature difference between hydrous and volatile-free melting at 3 – 4 GPa has been suggested, though not confirmed, to be in the order of 1000 °C (refs 15,16). As a consequence, the temperature breakdown of hydrous silicates in the presence of carbonates in Ca-enriched compositions should be factors promoting the generation of liquids fractionating large quantities of volatiles.

The pattern of devolatilization for subducted igneous crust has been mostly assessed in a limited range of bulk compositions, i.e. for basalts at bulk normative anorthite content (*An*) from 23 to 32 wt.% (Supplementary Table S1). The mafic crust however includes several km-thick sequences of gabbros and troctolites, with up to 80% modal plagioclase, and *An* ranging from 30 to 70%, as sampled in the Pacific[17], Atlantic[18], and Indian[19] oceans'. The alteration of plutonic rocks is documented by the precipitation of calcite and of Ca-Al-silicates with mafic hydrates down to depths of 1500 meters below seafloor, leading to relatively high bulk CO_2 contents, locally up to 8 wt.%[20]. Fluid-rock interaction may act at much greater depths, e.g. along faults at the outer rise outboard of trenches[21]. Upon subduction, epidote is the hydroxylated Ca-Al-silicate then responsible for the ultimate dehydration of the mafic slab at sub-arc depth; its abundance and pressure stability are promoted by high bulk normative anorthite contents[22]. Devolatilization of altered gabbros at high pressures is unexplored and the features of liquids released by decomposition and/or dissolution of carbonates and epidote are unknown.

I conducted high-pressure experiments (see Methods) on a variably hydrated and carbonated model gabbro (Supplementary Table S1), An_{44}, in order to evaluate the nature of the liquids formed

from carbonate dissolution or melting. The experiments were designed based on a conceptual model developed in the model system CaO-CO_2-H_2O (Supplementary Methods S1 and Fig. S1). Synthesis experiments were performed from 3.7 to 4.6 GPa, and from 700 °C to 1000 °C. In order to constrain the composition of the liquids, sandwich experiments were performed at 4.2 GPa, and variable CO_2:H_2O ratio.

Garnet, omphacite, and coesite are observed in all experiments (Supplementary Table S2). Lawsonite forms with dolomite and magnesite at low temperature, up to 750 °C at 3.7 GPa. At temperatures exceeding lawsonite stability, kyanite is always present as a result of the model dehydration reaction lawsonite = zoisite + kyanite + coesite + H_2O. Epidote crystallizes up to 3.8 GPa, with dolomite and magnesite.

The key observation in the first two sets of experiments is the occurrence of peculiar microstructures observed at 900 °C, 3.8 – 4.2 GPa (Fig. 1a-b, and Supplementary Fig. S2). The carbonate phase in H_2O-poor experiments at 900 °C displays lobes and cusps, it often includes sub-spherical inclusions of a silica-rich phase, and it forms feathery grain boundaries at contacts with garnet and clinopyroxene. Electron microprobe analysis reveals that the carbonate phase contains approximately 40 wt.% CaO, 5 wt.% FeO, 4 wt.% MgO and 2.3 wt.% Na_2O (Supplementary Table S3); and that subspherical silicate inclusions have tonalitic-trondhjemitic composition. Lobe and cusp structures are known to develop during viscous fingering moved by Saffman-Taylor instabilities in liquids of contrasting viscosities, whereas growth of feathery solids is related to crystallization of highly undercooled liquids. Rounded, spherical boundaries between a carbonate and a silicate phase have been regarded as immiscibility features. All of these observations therefore strongly support the occurrence of more than a single liquid phase upon quenching of experimental charges at 900 °C. Experiment at 4.0 GPa, 870 °C shows that epidote is absent and that the carbonates are euhedral aragonite and a dendritic Mg-calcite, suggesting that a liquid may have occurred even at lower temperature.

Whether such liquids and a vapor (Supplementary Methods S1) coexisted at run conditions or they exsolve from a single liquid it cannot be resolved from the microstructures observed in these experiments. I therefore designed a geometry for a new set of experiments where a carbonate layer is sandwiched within the model gabbro gel powder (see Methods). The carbonate layer has the same composition of the putative carbonate-silicate liquid retrieved from the "forward" experiments described above. The sandwich experiment at 850 °C, 4.2 GPa produced aragonite and dolomite coexisting with the eclogitic assemblage. Macroscopic observation of the run charge reveals a diffuse porosity (Supplementary Fig. S3a), more pronounced at the top of the capsule, where sub-spherical droplets of a carbonate phase were recognized, therefore suggesting that dissolution of carbonate is conspicuous (Supplementary Fig. S3b). Experiments at 900 °C, 4.2 GPa, were run at variable CO_2:H_2O ratio and always produced a solid assemblage consisting of garnet, omphacite, kyanite, aragonite plus a complex intergrowth of Ca-carbonate dendrites and tonalitic glass as a froth or as droplets (Fig. 1c and 1d, Supplementary Fig. S3d), delimited by a well-defined meniscus at the hot portion of the run charge (Supplementary Fig. S3c). Minor Na-carbonate was recognized along grain boundaries (Supplementary Fig. S4). Vesicles are homogeneously distributed in the carbonate-silicate intergrowth, they are micrometric to sub-micrometric in size, and more abundant in the center of silicate glass globules; I found no evidence of large spherical vesicles, which can be attributed to a coexisting vapor phase (see Supplementary Methods S4). Such textural features can be interpreted as a precipitation sequence upon quenching of a single volatile rich liquid, although the appearance of a liquid and vapor is possible at very large CO_2:H_2O ratio (e.g. in experiment with 0.4 wt.% H_2O and 13.4 wt.% CO_2; see point 2 in Supplementary Fig S1b). The carbonate layer is entirely liquefied at 3.7 wt% H_2O, so the amount of H_2O dissolved in the liquid can be calculated from image analysis of quenched products. Although a correct assessment of the silicate/carbonate proportion in the hydrous carbonate liquid is at present unfeasible, results give ~20 wt.% H_2O and ~25 wt.% CO_2.

Because carbonate precipitates first upon quenching, FeO, MgO, and CaO are fractionated in the carbonate dendrite. Therefore the ratio between these oxides can be used as a proxy for the compositional features of the original carbonatitic liquids, which in both forward and sandwich experiments Ca-rich, X_{Ca} ~ 0.8 (X_{Ca} = Ca/(Ca+Fe+Mg), Fig 2a). When compared to carbonatitic liquids obtained from other mafic eclogites, Ca-enriched hydrous carbonatitic liquids obtained in this study are similar to liquids obtained from starting materials bearing minor H_2O[14,23], whereas liquids from anhydrous melting[10,13] are displaced to much lower X_{Ca}, down to X_{Ca} = 0.5. Notably, despite much lower normative anorthite of bulk composition used in previous studies[14,23], the coexisting solid carbonate is either aragonite or Mg-calcite, when H_2O is present.

Ternary, (Ca, Mg, Fe)-carbonates are the major components of carbonatitic liquids observed in a variety of geodynamic settings, nonetheless knowledge of the liquidus surface is limited to binary systems. On the Ca-Mg join[16], the topology of the dry liquidus (Fig 2b) is characterized by the peritectic reaction involving dolomite, at T ~ 1400 °C and P ~ 3 GPa, and by a minimum at 1300–1350 °C, X_{Ca} ~ 0.6. At such temperatures, carbonate liquids at anhydrous conditions precipitate a single carbonate solid solution. At wet conditions, the liquidus surface is profoundly depressed to lower T at the $CaCO_3$ vertex[15]; consequently the minimum melting is expected to shift toward Ca-rich compositions. In this region, the calculated ternary phase diagram at T<900 °C shows the presence of two and three phase fields (Fig 2b) in the subsolidus. Therefore, the appearance of a liquid occurs along a eutectic reaction, where the carbonate liquid coexists with two solid carbonates, fading to a minimum when, similarly to ternary feldspars, a single solid carbonate forms. The schematic projection of the liquidus surface in Fig. 2b therefore provides the basis for understanding the common compositional character of hydrous carbonatitic liquids from various mafic eclogites, as well as predicting melt compositions from impure marbles flushed by hydrous solutions.

Previous studies on hydrous carbonated eclogites[9,14,23,24,25] show that liquids on the solidus are invariably silicate at shallow depth, independent of the CO_2:H_2O ratio in the starting material.

Although dissolution of CO_2 in a silicate melt has been suggested on the basis of mass-balance constraints[24], no direct evidence of quenched carbonatitic liquids was found at temperatures below 1020-1100 °C in basaltic eclogites (dry[13] and wet[14]), and at 1070 °C in pelitic carbonated eclogites[9]. I therefore suggest here that the high X_{Ca} and *An* in the bulk composition drive the production of large proportions of carbonate component in hydrous liquids at temperatures as low as 870-900 °C. These temperature conditions, at pressures of 3.8-4.2 GPa, are encountered by the top of a subducting slab (Fig. 3) in a warm thermal regime[26], if a H_2O source is provided. Such a source may correspond to hydrous solutions flushed from the underlying dehydrating serpentinized lithosphere or to an internal source, i.e. epidote, as shown here.

The mobile carbonatitic liquid, enriched in Ca, Si, and volatiles, would percolate into the harzburgitic mantle wedge and reacts with olivine to generate clinopyroxene, magnesite, and eventually amphibole at pressures below 3 GPa[8]. A layer of variably hydrated magnesite-lherzolite/pyroxenite can be expected to form first at the hanging wall of the slab; entrainment of this hybridized composition in the wedge at temperatures exceeding 950-1000 °C [8,29] will generate a derivate hydrous carbonate-silicate liquid, where the carbonate component shifts to dolomitic composition. Migrating upwards in the hottest portion of the wedge, where large batches of arc-magmas are produced, hydrous-carbonatitic liquids will dilute, mimicking a pyroxenite signature. This process will be most effective on warm active margins: for example, the exceptionally high CO_2 content of undegassed melts reconstructed for the Andes[4] could be correlated to the gabbroic rocks produced at East Pacific Rise and to thick pelagic limestones sedimented on the Nazca plate[30].

Methods

Plutonic sections of the oceanic crust include suites of olivine gabbros and troctolites. The composition of olivine gabbro 59-3 (ref. 19, Supplementary Table S1) was used as a reference, with 63 % modal plagioclase and 33 % modal clinopyroxene.

The first set of experiments (bulk composition 59-3, Supplementary Methods S2 and S3, Supplementary Table S2) was aimed to verify the pressure stability of epidote and the location of first appearance of vapor-saturated silicate liquids, following an experimental procedure described previously[7], using a conventional double capsule technique. H_2O and CO_2 were added by oxalic acid dihydrate, which provides a source of volatiles decoupled from chemical variations of non-volatile components. The reactions governing the subsolidus phase relationships in vapor-bearing basaltic compositions at high pressure[7] provided the frame to plan the experimental investigation. The maximum and the minimum fraction of CO_2 in the vapor was estimated by thermodynamic calculations (Supplementary Methods S3) assuming either the precipitation of graphite in a COH vapor or a binary H_2O-CO_2 mixture in equilibrium with zoisite, aragonite, kyanite and coesite. Upper and lower bounds provide a rough estimate of fractions of H_2O and CO_2 feasible.

The second set of experiments (Supplementary Table S2, bulk composition 59-3 ccb) was intended to reproduce vapor-poor or vapor-absent conditions, assuming that carbonate, epidote, and eventually liquid, fractionate most volatile components in this Ca-rich starting material. In order to match the chemical and mineralogical composition of altered gabbros, e.g. as recorded in ODP Hole 735B (sample A1-2, ref. 20), the precipitation of secondary minerals was modelled by the addition of 11 wt.% calcite (cc) and 1.24 wt.% brucite (br). Differences in the composition of natural sample A1-2 and of starting material 59-3ccb as compared to 59-3 are expected to produce a higher amount of carbonate in the run products without altering phase relationships of silicates, in the range of pressure and temperature investigated here. A single Au capsule was used for these runs.

A third set of experiments was introduced after the discovery of textures suggesting the occurrence of carbonatitic liquids formed in the first two sets of experiments. In this third set, “reverse”, synthesis experiments were produced by a sandwich technique where a carbonate layer

was inserted in 1:5 proportion between two layers of the same gel used for the previous, “forward”, experiments. The composition of the carbonate layer is based on the composition of carbonate quench products in forward experiment at 900 °C, 4.2 GPa (Supplementary Table S3), adjusted to obtain positive mass balance of all run products. Because all synthesis performed in forward experiments above lawsonite field contain kyanite, precise amounts of H_2O in the run charge can be obtained by adding a bottom layer of $Al(OH)_3$ and SiO_2, which produce kyanite + H_2O at run conditions. Although the bulk composition of the entire run charge is different from 59-3 and 59-3ccb, such difference simply accounts for a larger proportion of the putative hydrous-carbonatitic liquid formed and of kyanite. At equilibrium, therefore, the chemical potential of components investigated in this study is identical to 59-3ccb, whereas phase proportions vary, in order to facilitate analytical characterization. In summary, this approach does not differ from experimental studies varying the amount of olivine or silica, in olivine- or silica-saturated systems. Three experiments at variable CO_2:H_2O ratio (33, 10, and 2.7, Supplementary Table S2) were performed, in order to estimate if variation in volatiles affect the appearance of two distinct liquid phases (e.g. “vapor” and “liquid”, Supplementary Methods S1, Fig. S1).

An end-loaded piston cylinder apparatus was used for experiments to pressures of 3.8 GPa, and a Walker-type multi-anvil for pressures at or above 4.0 GPa. Run products were characterized by electron-microprobe analyses, on a Jeol JXA 8200 equipped with five wavelength-dispersive spectrometers. Analyses were conducted at conditions of 15 kV and 5 nA. Analytical details are given in ref. 8.

The demonstration of the identity of equilibrium chemical potentials in forward and sandwich experiments relies on the verification of identity in solid phase assemblage and mineral composition at variable phase proportions in the two approaches. Despite the large difference in the bulk CaO content of the experimental charge, due to the different proportions in carbonates and silicates, we obtained identical X_{Ca} and X_{Mg} ratios (X_{Ca} = Ca/(Ca+Fe+Mg)) in forward and sandwich

experiments for both garnet and clinopyroxene (Supplementary Table S3) indicating that the composition of liquids identified is valid for gabbroic eclogites.

References

1. Burton, M. R., Sawyer, G. M. & Granieri, D. Deep Carbon Emissions from Volcanoes. *Rev. Mineral. Geochem.* **75**, 323-354 (2013).
2. Hilton, D.R., Fischer, T.P. & Marty, B. Noble gases and volatile recycling at subduction zones. *Rev. Mineral. Geochem.* **47**, 319-370 (2002).
3. Dasgupta, R. & Hirschmann, M.M. The deep carbon cycle and melting in Earth's interior. *Earth Planet. Sci Lett.* **298**, 1-13 (2010).
4. Fischer, T.P. & Marty, B. Volatile abundances in the sub-arc mantle: insights from volcanic and hydrothermal gas discharges. *J. Volcan. Geotherm. Res.* **140**, 205–216 (2005).
5. Schmidt, M.W. & Poli, S. Devolatilisation During Subduction. *Treatise on Geochemistry* **4**, 669-701 (2014).
6. Gorman, P.J., Kerrick, D.M. & Connolly, J.A.D. Modeling open system metamorphic decarbonation of subducting slabs. Geochem. Geophys. Geosys. **7**, Q04007 (2006).
7. Poli S., Franzolin E., Fumagalli P. & Crottini A. The transport of carbon and hydrogen in subducted oceanic crust: an experimental study to 5 GPa. *Earth Planet. Sci Lett.* **278**: 350-360 (2009).
8. Tumiati S., Fumagalli P., Tiraboschi C. & Poli S. An experimental study on COH-bearing peridotite up to 3.2 GPa and implications for crust-mantle recycling. *J. Petrology* **54**, 453-479 (2013).
9. Grassi, D. & Schmidt, M.W. The Melting of Carbonated Pelites from 70 to 700 km Depth. *J. Petrology* **4**, 765-789 (2011).
10. Yaxley, G.M. & Brey, G.P. Phase relations of carbonate-bearing eclogite assemblages from 2.5 to 5.5 GPa: implications for petrogenesis of carbonatites. *Contrib. Mineral. Petrol.* **146**,

606-619 (2004).

11. Manning, C. E., Shock, E. L. & Sverjensky, D. A. The chemistry of carbon in aqueous fluids at crustal and upper-mantle conditions: Experimental and theoretical constraints. *Rev. Mineral. Geochem.* **75**, 109–148 (2013).
12. Ague, J. J. & Nicolescu, S. Carbon dioxide released from subduction zones by fluid-mediated reactions. *Nature Geosci.* **7**, 355-360 (2014).
13. Dasgupta, R., Hirschmann, M.M. & Withers, A.C. Deep global cycling of carbon constrained by the solidus of anhydrous, carbonated eclogite under upper mantle conditions. *Earth Planet. Sci Lett.* **227**, 73-85 (2004).
14. Kiseeva, E.S., Yaxley, G.M., Hermann, J., Litasov, K.D., Rosenthal, A. & Kamenetsky, V.S. An Experimental Study of Carbonated Eclogite at 3 center dot 5-5 center dot 5 GPa-Implications for Silicate and Carbonate Metasomatism in the Cratonic Mantle. *J. Petrology* **53**, 727-759 (2012).
15. Wyllie, P.J. & Boettcher, A.L.. Liquidus phase relationships in the system CaO-CO_2-H_2O to 40 kilobars pressure with petrological applications. *Am. J. Sci.* **267-A**, 489-508 (1969).
16. Irving, A.J. & Wyllie, P.J. Subsolidus and melting relationships for calcite, magnesite and the join $CaCO_3$-$MgCO_3$ to 36kb. *Geochim. Cosmochim. Acta* **39**, 35-53 (1975).
17. Perk, N.W., Coogan, L.A., Karson, J.A., Klein, E.M., Hanna, H.D. Petrology and geochemistry of primitive lower oceanic crust from Pito Deep: implications for the accretion of the lower crust at the Southern East Pacific Rise. *Contrib. Mineral. Petrol.* **154**, 575-590 (2007).
18. Godard, M., Awaji, S., Hansen H., Hellebrand E., Brunelli D., Johnson K., Yamasaki T., Maeda J., Abratis M., Christie D., Kato Y., Mariet C., Rosner M. Geochemistry of a long in-situ section of intrusive slow-spread oceanic lithosphere: Results from IODP Site U1309 (Atlantis Massif, 30°N Mid-Atlantic-Ridge). *Earth Planet. Sci Lett.* **279**, 110–122 (2009).
19. Meyer, P.S., Dick, H.J.B. & Thompson, G. Cumulate gabbros from the Southwest Indian

Ridge, 54° S – 7°16' E: implications for magmatic processes at slow spreading ridge. *Contrib. Mineral. Petrol.* **103**, 44-63 (1989).

20. Bach, W., Alt, J.C., Niu, Y.L., Humphris, S.E., Erzinger, J., Dick, H.J.B. The geochemical consequences of late-stage low-grade alteration of lower ocean crust at the SW Indian Ridge: Results from ODP Hole 735B (Leg 176). *Geochim. Cosmochim. Acta* **65**, 3267-3287 (2001).
21. Ranero, C.R., Phipps Morgan, J., McIntosh, K. & Reichert C. Bending-related faulting and mantle serpentinization at the Middle America trench. *Nature* 425, 367-373 (2003).
22. Poli, S., Schmidt, M.W. Experimental subsolidus studies on epidote minerals. Epidotes. *Rev. Mineral. Geochem*. **56**: 171-195 (2004).
23. Hammouda, T. High-pressure melting of carbonated eclogite and experimental constraints on carbon recycling and storage in the mantle. *Earth Planet. Sci Lett.* **214**, 357-368 (2003)
24. Tsuno, K. & Dasgupta, R. The effect of carbonates on near-solidus melting of pelite at 3 GPa: Relative efficiency of H_2O and CO_2 subduction. *Earth Planet. Sci Lett.* **319-320**, 185-196 (2012).
25. Yaxley, G. & Green, D.H. Experimental demonstration of refractory carbonate-bearing eclogite and siliceous melt in the subduction regime. *Earth Planet. Sci Lett.* **128**, 313-325 (1994).
26. Syracuse, E. M., van Keken, P. E. & Abers, G. A. The global range of subduction zone thermal models. *Phys. Earth Planet. Inter.* **183**, 73–90 (2010).
27. Connolly, J. A. D. Multivariable phase diagrams: An algorithm based on generalized thermodynamics, *Am. J. Sci.* **290**, 666–718 (1990)
28. Franzolin E., Schmidt M.W. & Poli S. Ternary Ca–Fe–Mg carbonates: subsolidus phase relations at 3.5 GPa and a thermodynamic solid solution model including order/disorder. *Contrib. Mineral. Petrol.* **161**, 213-227 (2011).

29. Wallace, M. E. & Green, D. H. An experimental determination of primary carbonatite magma composition, *Nature* **335**, 343-345 (1988).
30. Plank, T. The Chemical Composition of Subducting Sediments, *Treatise on Geochemistry* **4**, 607-629 (2014).

Acknowledgements: I thank D.H. Green, M.W. Schmidt, N. Malaspina, P. Fumagalli, S. Tumiati, T. Hammouda, J. Hermann for fruitful discussions on the petrology of subduction zones. E. Erba introduced me to the world of pelagic sediments. A. Risplendente is acknowledged for the assistance at the electron microprobe. Comments from T. John and an anonymous reviewer greatly improved the manuscript. Funding provided by the Italian program PRIN2012R33ECR.

Figure legends

Figure 1. BSE images of quenched hydrous carbonatitic liquids at 4.2 GPa, 900 °C in forward (a, b), and sandwich (c, d) experiments. Roman letters identify phases, whereas Greek letters stand for textures. Garnet (G), clinopyroxene (P), aragonite, kyanite, and coesite occur in both experiments. **a**, the Ca-rich, (Mg,Fe,Na)-bearing carbonate (C) precipitates upon quenching of forward experiments forming lobes (λ) and cusps (ξ). **b**, quench carbonate forms feathery (ϕ) boundaries at the contact with garnet and pyroxene, and rounded (o) boundaries in contact with a Si-Al-rich phase (R). **c**, quench carbonate in sandwich experiments forms rhombohedral dendrites (δ) hosting a froth of silicate glass (S). **d**, bubble-free rims of silicate glass coalesce with spherical droplets of the Si-Al-rich quench phase (R), last residue of the quenching sequence.

Figure 2. Liquid compositions in the ternary carbonate system (molar proportions). **a**, dry experiments[10,13] approach composition of dolomite s.s., whereas “wet” liquids (this study and refs

14, 23) are displaced to higher Ca contents. Numbers are keyed to reference list. **b**, Schematic arrangement of the dry peritectic (orange) and the minimum (red) on the liquidus surface is compared to the location of the wet cotectic (blue). Cotectic line fades into a divariant minimum where a single carbonate crystallizes from the liquid. Thermodynamic calculation[27] of near solidus (870 °C) relationships in non-ideal carbonates[28] are in black. Single carbonate phase fields are in grey, and dashed lines stand for equilibrium of two coexisting carbonates.

Figure 3. Reactions governing dehydration, vapor-absent melting, and generation of a hydrous carbonatitic liquid in an altered oceanic gabbro. Lawsonite is the H_2O reservoir (blue field) for cold thermal regimes in the subducted slab; H_2O and CO_2 are stored in hydrous silicates and carbonates, and transported to depth. At intermediate regimes, dehydration is governed by epidote (light blue field). For warm P-T paths, the altered intrusives intersect the epidote vapor-absent melting reaction (Supplementary Methods S5) generating a carbonatitic liquid. Textural features of experiments suggest that transition from aqueous vapor, rich in carbonate solute, to a hydrous carbonatitic liquid could be continuous at 4.2 GPa. (Mg,Fe)-calcite is stable with the carbonatitic liquid. Numbers in figure stand for reference number.

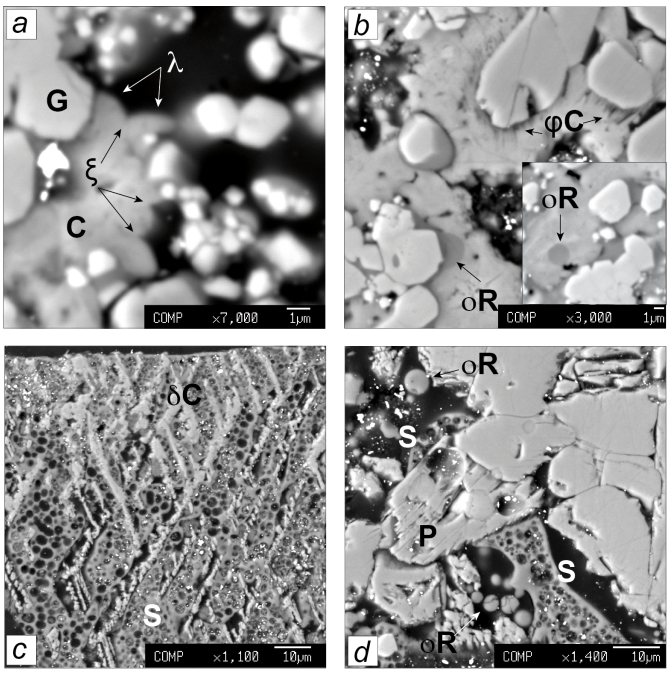
a
λ
G
ξ
C
COMP ×7,000 1μm
b
φC
oR
oR
COMP ×3,000 1μm
δC
S
c
COMP ×1,100 10μm
oR
S
P
S
oR
d
COMP ×1,400 10μm

Fig. 1

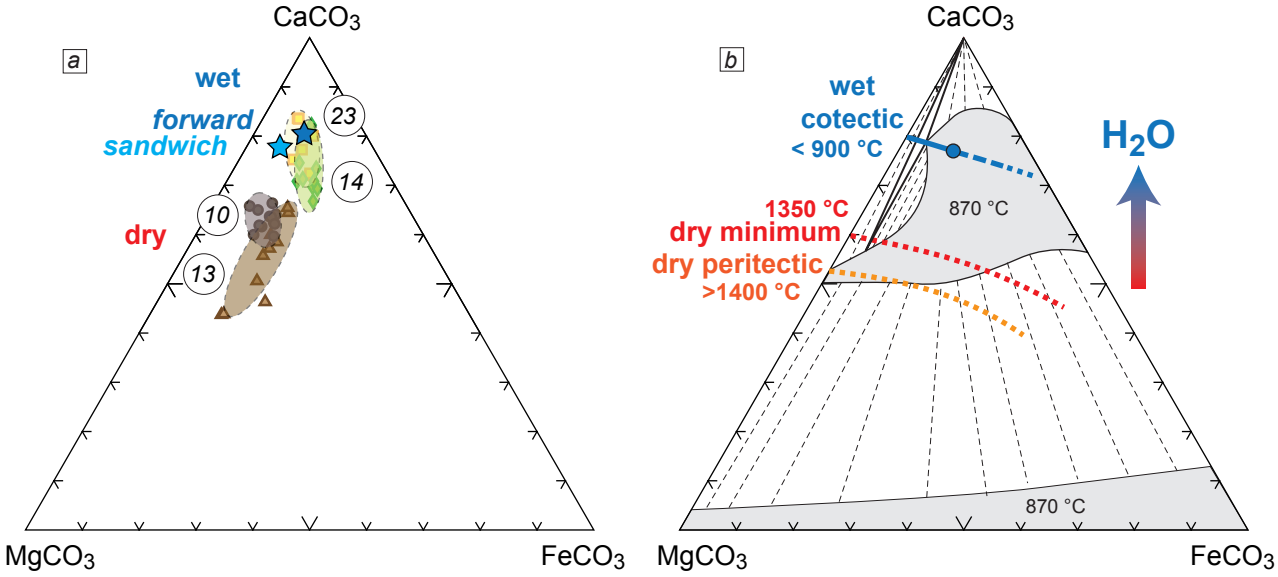
a
CaCO3
wet
forward
sandwich
23
14
10
dry
13
MgCO3
FeCO3
b
CaCO3
wet
cotectic
< 900 °C
H2O
1350 °C
dry minimum
dry peritectic
>1400 °C
870 °C
870 °C
MgCO3
FeCO3

Fig. 2

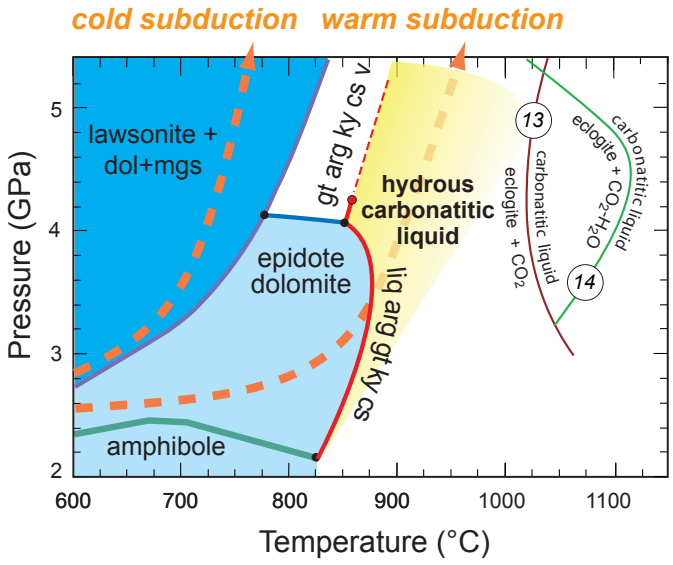
cold subduction
warm subduction
lawsonite +
dol+mgs
epidote
dolomite
amphibole
gt arg ky cs v
hydrous
carbonatitic
liquid
liq arg gt ky cs
13
14
carbonatitic liquid
eclogite + CO2
eclogite + CO2-H2O
carbonatitic liquid
Pressure (GPa)
Temperature (°C)
2
3
4
5
600
700
800
900
1000
1100

Fig. 3

Carbon mobilised at shallow depths in subduction zones by carbonatitic liquids

SUPPLEMENTARY INFORMATION

Included in this file are sections providing additional experimental details and References

SUPPLEMENTARY METHODS

S1. A conceptual model for investigating liquids in systems bearing Ca-carbonates and hydrous phases

The appearance of liquids at high pressure in chemical systems bearing both carbonates and hydrous phases is governed by the complex shapes of the "vaporous" and of the "liquidus" surfaces as theoretically investigated since the early '60s of the last century in the model system CaO-CO_2-H_2O (refs 1-3). It has been predicted[2] that the volatile-rich liquid (vapor) and the melt (non-volatile components rich liquid), may converge to form a single supercritical liquid at pressures higher than 4 GPa (Fig. S1a), although experimental data supporting this idea are scarce. H_2O solubility in carbonate liquids has been determined at low pressure only; however, 14 wt.% H_2O was found to dissolve in a Ca-Mg-Na liquids[4] at 0.22 GPa, a value two-three times larger than in silicate melts. The addition of silica and alkalis to the system is expected to further complicate the liquidus surface, because a carbonate liquid and a silicate liquid have been found to be partly immiscible[5,6]. Therefore two liquids and a vapor phase are potentially present in a silicate bulk rock composition bearing Ca-carbonates and hydrous phases at high temperature. For sake of simplicity, we neglect here the latter case and we use the system CaO-CO_2-H_2O as a conceptual model to plan the experimental investigation on the Ca-rich bulk compositions considered.

Figure S1a shows that the vapor-saturated liquidus and the liquid-saturated vaporous coalesce at relatively low temperatures. Supplementary Figure S1b is a hypothetical isothermal section constructed at temperatures in the order of 900-1000 °C, i.e. well above melting of the hydrous

phase portlandite, $Ca(OH)_2$, and therefore above the three minima of the ternary liquidus surface. At such conditions, different bulk compositions lead to the formation of one, two, and three phase assemblages. The bulk composition 1, in Fig. S1b, represented by the blue circle, at CO_2:H_2O ratio "x" will produce an assemblage composed of a carbonate and abundant single liquid, rich in non-volatile components. Any variation of volatile abundances in this two-phase field, where bulk 1 lies, will simply result in a variation of the proportion between solid and liquid, but it will not alter the location of the liquidus surface. The bulk composition 2, in red, at the same CO_2:H_2O ratio "x", will show a three phase assemblage, i.e. carbonate, a volatile-rich liquid (*a* in figure), and a vapor (*b*). The bulk composition in green (3) has a higher amount of volatiles available, higher total H_2O, but will give a "subsolidus" assemblage composed of carbonate and vapor, without "melt". The bulk composition 4, in orange, with CO_2:H_2O ratio "y", has a lower amount of volatiles available, gives a large proportion of carbonate, but produces a vapor-saturated "melt". The liquids formed at 1, 2, and 4 will follow liquid lines of descent forming a single supercritical liquid (*c* in Figure S1b) upon cooling, because supercritical behaviour (c) already occurs at the leading edge of the cotectic line (Figure S1a).

The experimental study illustrated in this contribution therefore moves from the idea of having relatively large bulk CO_2:H_2O ratios in order to stabilize a carbonate in a large range of P-T conditions. Then, different sets of total volatile components added in the starting material, and of variable CO_2:H_2O offer the opportunity to inspect the features of liquids formed. The first set of experiments, where oxalic acid di-hydrate (OAD) is used as a source of volatiles (Supplementary Table S2) corresponds to a case where CO_2:H_2O is relatively low (bulk composition 1 or 2 in Fig. S1b) and where the fraction of carbonates compared to silicates is low; the second set of experiments approaches condition 4; the third set, with a geometry of a "sandwich" run charge explores the variable CO_2:H_2O, i.e. how liquids change moving from 1 to 4.

S2. Bulk compositions and starting materials

Most experimental studies on the fate of crustal rocks at sub-arc depth focused either on altered oceanic basalts or on carbonated pelitic metasediments. The chemistry of altered MORBs has been used mostly as a reference, with Mg# (100*Mg/(Mg+Fe)) and *An* (CIPW normative anorthite) ranging from Mg# 47 and *An* 23 in ref. 7 to Mg# 64 and *An* 24 in ref. 8. However gabbros recovered from a variety of spreading centers, both in fast and slow spreading oceans, reveal sequences of plagioclase rich "cumulates" with Mg# up to 90, and, most importantly *An* to 70 (refs. 9, 10). Such variations in Ca, Al, Mg, and Fe are expected to profoundly modify the phase relations at high-pressure, including liquids and carbonates present when CO_2 is added to the system. The composition of an olivine gabbro from the Southwest Indian Ridge (sample 59-3, ref. 11, Supplementary Table S1) was used as a representative composition.

In order to promote the synthesis at subsolidus conditions, a gel of chemical composition corresponding to sample 59-3 (Table S1) has been prepared using tetraethylorthosilicate (TEOS) as silica source, pure Na-, Ca-, Mg- and Al- nitric solutions, and ferric benzoate for Fe_2O_3. Gels have the major advantage of a large active surface, and perfect homogeneity, related to the co-precipitation of a hydrogel from clear solutions. Gels were fired in a gas mixing furnace at fO_2 conditions approaching FMQ buffer at 1 atm, then seeded with 3 wt% of a mixture of garnets and clinopyroxene, that are expected to be major phases stable in the pressure range investigated. Individual seed composition (pyrope, almandine, grossular, diopside) largely differs from the stable composition expected at P-T conditions investigated to favour unquestionable identification of relicts, but the composition of seeds mixture closely reproduces the bulk composition chosen to avoid fractionation.

The precipitation of secondary minerals in mafic rocks[12] was reproduced adding reagent grade $CaCO_3$ and natural brucite to gel 59-3, leading to bulk composition 59-3 ccb (Supplementary Table S1).

The carbonate layer in sandwich experiments was prepared from reagent grade Na_2CO_3, $CaCO_3$, natural dolomite from Bazena (Adamello, Italy), and siderite from Ivigtut (Greenland) as starting materials. Stoichiometric proportions of $Al(OH)_3$ and amorphous SiO_2 were used to produce kyanite and H_2O.

S3. Hydrogen buffering and speciation in vapor-saturated experiments

A conventional double capsule technique[13] was adopted in experiments with bulk composition 59-3 (Table S1 and Table S2). Hydrogen fugacity was buffered by hematite-magnetite (HM) - H_2O mixture, using inner $Ag_{50}Pd_{50}$ capsules and outer Au capsules. Welded inner capsules (2 mm long) contain the starting materials plus 10 wt% oxalic acid dihydrate (OAD). It is worth introducing here that HM in the outer capsule fix the chemical potential of hydrogen in a pure H_2O vapor, but the inner capsule contains a mixed vapor; as a consequence the oxygen fugacity in the inner capsule is intrinsically lower than in the outer capsule (see details in ref. 14). The actual value of the oxygen fugacity in the inner capsule is then fixed either by redox equilibria, or by a fixed C:O ratio, or by the occurrence of graphite/diamond.

The precipitation of graphite in runs externally buffered by the HM equilibrium is theoretically possible. Because at high-pressure low-temperature conditions the graphite saturation boundary closely approaches the H_2O-CO_2 join (GCOH vapor), excess H drives the composition of OAD within the graphite + vapor field in a C-O-H diagram. Therefore, the maximum fraction of CO_2 in the inner capsule can be calculated assuming the precipitation of graphite. This condition is unlikely here as graphite was not detected, but gives an upper bound of vapor speciation. Alternatively, the absence of graphite at high pressure may suggest that the vapor lies on the H_2O-CO_2, and the minimum fraction of CO_2 in the vapor is then obtained for a binary mixture in equilibrium with zoisite, aragonite, kyanite and coesite.

The speciation of experimental vapors was computed using the routines “vertex” and “fluids” in the thermodynamic software package Perplex[15], by calculating first the fugacities of oxygen and

hydrogen as fixed by the equilibria HM-H_2O in the outer capsule. Then, I refined, in a graphite/diamond-saturated vapor, the X_O conditions ($X_O = n_O/(n_O+n_H)$, n_i number of moles of i) where the hydrogen fugacity attains the value as buffered by equilibrium HM. The estimated vapor compositions were always computed at X_O>1/3 and they show a progressive enrichment in H_2O species with increasing pressure. The maximum X_{CO2} (in the GCOH vapor), at 4.2 GPa, 900 °C, on the HM equilibrium is 0.81, at log fO_2 (OH, external capsule) = -6.9, and log fH_2 (OH) = 2.0, corresponding to log fO_2 -8.5 in the inner capsule. The minimum X_{CO2} (H_2O-CO_2 vapor), at 4.2 GPa, 900 °C in equilibrium with a zoisite- aragonite- bearing assemblage (see also fig 7 in ref. 16) is 0.15.

S4. Microstructural features of liquids quenched at high pressure and the definition of dissolution and melting.

The interpretation of microstructure of quenched products bearing liquids at run conditions heavily relies on seminal works in the '70s, notably refs. 17, 18, and 19, the latter for hydrous systems. Dendrites form at large undercooling steps, and they have been observed in carbonates since the early work on calcite + H_2O (ref. 20). Spherulites and spherical droplets are typically associated to precipitation of partly or entirely amorphous solid after unmixing of a hydrous vapor phase during quench (e.g. microstructures reported in ref. 19, his Fig. 10). Quenched solute rich vapors are expected to bear fundamental analogies with hydrogels, characterized by a colloidal network, where spherules of insoluble particles are suspended in the liquid.

Carbonate liquids are known to have very low viscosities[21]. As a consequence, a coexisting vapor phase, when present during experiments, tends to coalesce in a few large bubbles (as shown in ref. 22, their Fig. 2d; in ref. 6, their Fig. 5a; ref. 23, their Fig 2i) leaving a limited number of large sub-spherical pores in run products after quenching. On the contrary vapors generated upon cooling, from unmixing of a single liquid at high temperature, form diffuse minute pores.

On the basis of this knowledge, quench microstructures observed in runs at 4.2 GPa, 900 °C, in

both forward and sandwich geometry, at variable H_2O content from 0.4% to 3.7 wt%, are interpreted to have a single volatile rich liquid at run condition (Fig. 1c and d, and Fig. S3c and d). Because carbonatitic liquids cannot be vitrified, carbonate dendrites precipitate first; a free vapor phase, solute-rich, separates from the silicate "residual" liquid afterwards, leaving a froth of tonalitic glass; progression of quenching is finally responsible for the precipitation of the solute from the vapor in the form of silica-rich droplets and Na-carbonate. Chemical composition of silicate glass (Table S3), consistently with the sequence proposed, is lower in silica compared to spherical droplets, which precipitate as ultimate products.

S5. Schreinemakers' analysis of phase relations

We showed here that epidote is a feasible internal H_2O reservoir up to 4 GPa in altered gabbros and that liquids form at 900 °C. The Schreinemakers' analysis in the system CaO-Al_2O_3-SiO_2-H_2O (ref. 24) serves as a basis for the arrangement of reactions involving garnet, dolomite, aragonite, epidote, silica, vapor and liquid. Subsolidus epidote breakdown with pressure is governed by the model reaction 6 zoisite + 6 dolomite = 12 aragonite + 4 garnet (gr_{50}) + 2 kyanite + 4 coesite + 3 H_2O in the system CaO-MgO-Al_2O_3-SiO_2-H_2O-CO_2 (CMASHC). The composition of the carbonate phase from quenched liquids and of the silicate glass provides a constrain for the composition of the liquid in a Schreinemakers analysis of the system CMASHC. Above 4 GPa (Fig. 3), vapor-saturated liquid forms by the reaction aragonite + dolomite + kyanite + quartz + vapor = liquid + garnet, whereas below 4 GPa, the epidote (zoisite) vapor-absent melting reaction is dolomite + zoisite = liquid + aragonite + garnet + kyanite + coesite, stoichiometric coefficients being a function of liquid composition, notably of his H_2O content.

REFERENCES FOR SUPPLEMENTARY METHODS AND TABLES

1. Wyllie, P.J. & Tuttle, F. The system CaO-CO_2-H_2O and the origin of carbonatites. *J. Petrol.* **1**, 1-46 (1960).

2. Wyllie, P.J. & Boettcher, A.L.. Liquidus phase relationships in the system $CaO-CO_2-H_2O$ to 40 kilobars pressure with petrological applications. *Am. J. Sci.* **267-A**, 489-508 (1969).
3. Boettcher, A.L. & Wyllie, P.J. The system $CaO-SiO_2-CO_2-H_2O$ – III. Second critical end-point on the melting curve. *Geochim. Cosmochim. Acta* **33**, 611-632 (1969).
4. Keppler, H. Water solubility in carbonatite melts. *Am. Mineral.* **88**, 1822–1824 (2003).
5. Freestone, I.C. & Hamilton, D.L. The role of liquid immiscibility in the genesis of carbonatites – An experimental study. *Contrib. Mineral. Petrol*. **73**, 105-117 (1980).
6. Martin, L.H.J., Schmidt, M.W., Mattsson, H.B., Guenther, D. Element Partitioning between Immiscible Carbonatite and Silicate Melts for Dry and H2O-bearing Systems at 1-3 GPa. *J. Petrol.* **54**, 2301-2338 (2013).
7. Forneris, J.F., Holloway, J.R. Phase equilibria in subducting basaltic crust: implications for H2O release from the slab. *Earth. Planet. Sci. Lett*. **214**, 187-201 (2003).
8. Dasgupta, R., Hirschmann, M.M. & Dellas, N. The effect of bulk composition on the solidus of carbonated eclogite from partial melting experiments at 3 GPa. *Contrib. Mineral. Petrol.* **149**, 288-305 (2005).
9. Perk, N.W., Coogan, L.A., Karson, J.A., Klein, E.M., Hanna, H.D. Petrology and geochemistry of primitive lower oceanic crust from Pito Deep: implications for the accretion of the lower crust at the Southern East Pacific Rise. *Contrib. Mineral. Petrol.* **154**, 575-590 (2007).
10. Godard, M., Awaji, S., Hansen H., Hellebrand E., Brunelli D., Johnson K., Yamasaki T., Maeda J., Abratis M., Christie D., Kato Y., Mariet C., Rosner M. Geochemistry of a long in-situ section of intrusive slow-spread oceanic lithosphere: Results from IODP Site U1309 (Atlantis Massif, 30°N Mid-Atlantic-Ridge). *Earth Planet. Sci Lett.* **279**, 110–122 (2009).
11. Meyer, P.S., Dick, H.J.B. & Thompson, G. Cumulate gabbros from the Southwest Indian Ridge, 54° S – 7°16' E: implications for magmatic processes at slow spreading ridge. *Contrib. Mineral. Petrol.* **103**, 44-63 (1989).
12. Bach, W., Alt, J.C., Niu, Y.L., Humphris, S.E., Erzinger, J., Dick, H.J.B. The geochemical

consequences of late-stage low-grade alteration of lower ocean crust at the SW Indian Ridge: Results from ODP Hole 735B (Leg 176). *Geochim. Cosmochim. Acta* **65**, 3267-3287 (2001).

13. Eugster, H.P., Skippen, G.B. Igneous and metamorphic reactions involving gas equilibria. In: Abelson P.H. (Ed), *Researches in geochemistry*, 492-450 (1967).
14. Poli S., Franzolin E., Fumagalli P. & Crottini A. The transport of carbon and hydrogen in subducted oceanic crust: an experimental study to 5 GPa. *Earth Planet. Sci Lett.* **278**: 350-360 (2009).
15. Connolly, J. A. D. Multivariable phase diagrams: An algorithm based on generalized thermodynamics, *Am. J. Sci.* **290**, 666–718 (1990).
16. Poli, S., Schmidt, M.W. The high-pressure stability of zoisite and phase relationships of zoisite-bearing assemblages. *Contrib. Mineral. Petrol*. **130**, 162-175 (1998).
17. Donaldson, C.H. An experimental investigation of olivine morphology. *Contrib. Mineral. Petrol*. **57**, 187-213 (1976).
18. Lofgren, G. An experimental study of plagioclase crystal morphology: isothermal crystallization. *Am. J. Sci.* **274**, 243-273 (1974)
19. Fenn, P.M. The nucleation and growth of alkali feldspars from hydrous melts. *Canadian Mineral.* **16**, 135-161 (1977)
20. Paterson, M. S. The melting of calcite in the presence of water and carbon dioxide. *Am. Mineral*. **43**, 603-606 (1958).
21. Treiman, A. H. Carbonatite magma: properties and processes. In: Bell, K. (ed.) Carbonatites: Genesis and Evolution. London: Unwin & Hyman, 89-104 (1989).
22. Thomsen, T. B. & Schmidt, M. W. Melting of carbonated pelites at 2.5-5.0 GPa, silicate-carbonatite liquid immiscibility, and potassium-carbon metasomatism of the mantle. *Earth Planet. Sci. Lett.* **267**, 17-31 (2008).
23. Tsuno, K. & Dasgupta, R. The effect of carbonates on near-solidus melting of pelite at 3 GPa: Relative efficiency of H_2O and CO_2 subduction. *Earth Planet. Sci Lett*. **319-320**, 185-196

(2012).

24. Poli, S., Schmidt, M.W. Experimental subsolidus studies on epidote minerals. Epidotes. *Rev. Mineral. Geochem*. **56**: 171-195 (2004).
25. Hammouda, T. High-pressure melting of carbonated eclogite and experimental constraints on carbon recycling and storage in the mantle. *Earth Planet. Sci Lett.* **214**, 357-368 (2003).
26. Kiseeva, E.S., Yaxley, G.M., Hermann, J., Litasov, K.D., Rosenthal, A. & Kamenetsky, V.S. An Experimental Study of Carbonated Eclogite at 3 center dot 5-5 center dot 5 GPa-Implications for Silicate and Carbonate Metasomatism in the Cratonic Mantle. *J. Petrology* **53**, 727-759 (2012).
27. Yaxley, G.M. & Brey, G.P. Phase relations of carbonate-bearing eclogite assemblages from 2.5 to 5.5 GPa: implications for petrogenesis of carbonatites. *Contrib. Mineral. Petrol.* **146**, 606-619 (2004).

Carbon mobilised at shallow depths in subduction zones by carbonatitic liquids

SUPPLEMENTARY INFORMATION

Included in this file are sections providing 4 Figures and 3 Tables

SUPPLEMENTARY FIGURES

Figure S1. The system CaO-CO_2-H_2O at pressures higher than 4 GPa, after ref. 2. a) projection of the liquidus surface; shaded fields indicate coexistence of vapor and liquid. b) hypothetical isothermal section at 900-1000 °C; shaded field stands for the single liquid present; tie-lines indicate coexisting phase compositions; 1-4 are different bulk compositions discussed in Supplementary Methods S1.

Figure S2. X-ray maps of a) Ca, b) Na, and c) Si in experiment SPT5, at 900 °C, 4.2 GPa. Warm colors stand for high concentration of element mapped. Ca fractionates preferentially in carbonate, Na in clinopyroxene, Si in an interstitial amorphous phase.

Figure S3. Backscattered electron images of representative experiments where either a "vapor" (single volatile-rich liquid) or a "melt" (non-volatile component rich liquid) occurs at run conditions. a) run SPT9, 4.2 GPa 850 °C, top of the capsule is on the right side; b) detail of particles precipitated in the porosity; arrows indicate sub-spherical droplets of a Ca-carbonate (C). c) run SPT10, 4.2 GPa 900 °C, 3.6 wt.% H_2O, top of the capsule is on the left side; note that dendrites and foamy glass are delimited by a well-defined meniscus toward a garnet rich layer. d) run SPT10, 4.2 GPa 900 °C, 0.4 wt.% H_2O; P is clinopyroxene, C is dendritic Ca-carbonate, S are droplets of tonalitic glass.

Figure S4. False color map based on Ca, Na and Si concentrations. Red is related to Ca content and indicates carbonate phases (C); yellow indicates Na-carbonates (N) in interstices; green is for silicates, garnet (G), clinopyroxene (P), glass (S) and the spherical droplets of residual (R) amorphous phase.

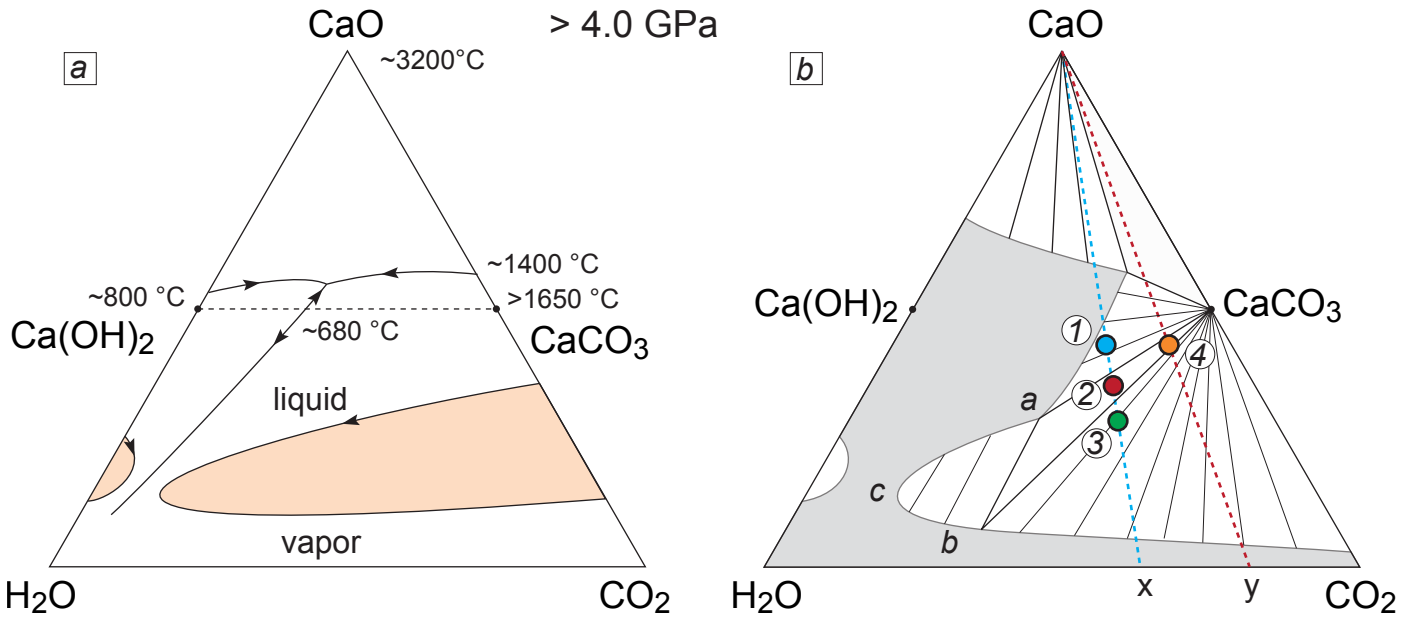
a
CaO
> 4.0 GPa
~3200°C
~1400 °C
~800 °C
>1650 °C
~680 °C
Ca(OH)2
CaCO3
liquid
vapor
H2O
CO2
b
CaO
Ca(OH)2
CaCO3
1
2
3
4
a
b
c
x
y
H2O
CO2

Fig. S1

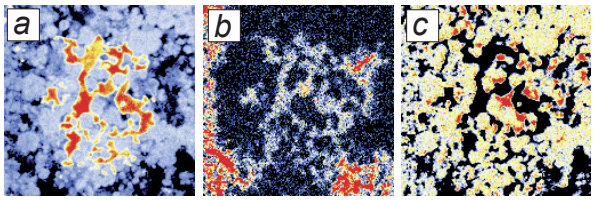

Fig. S2

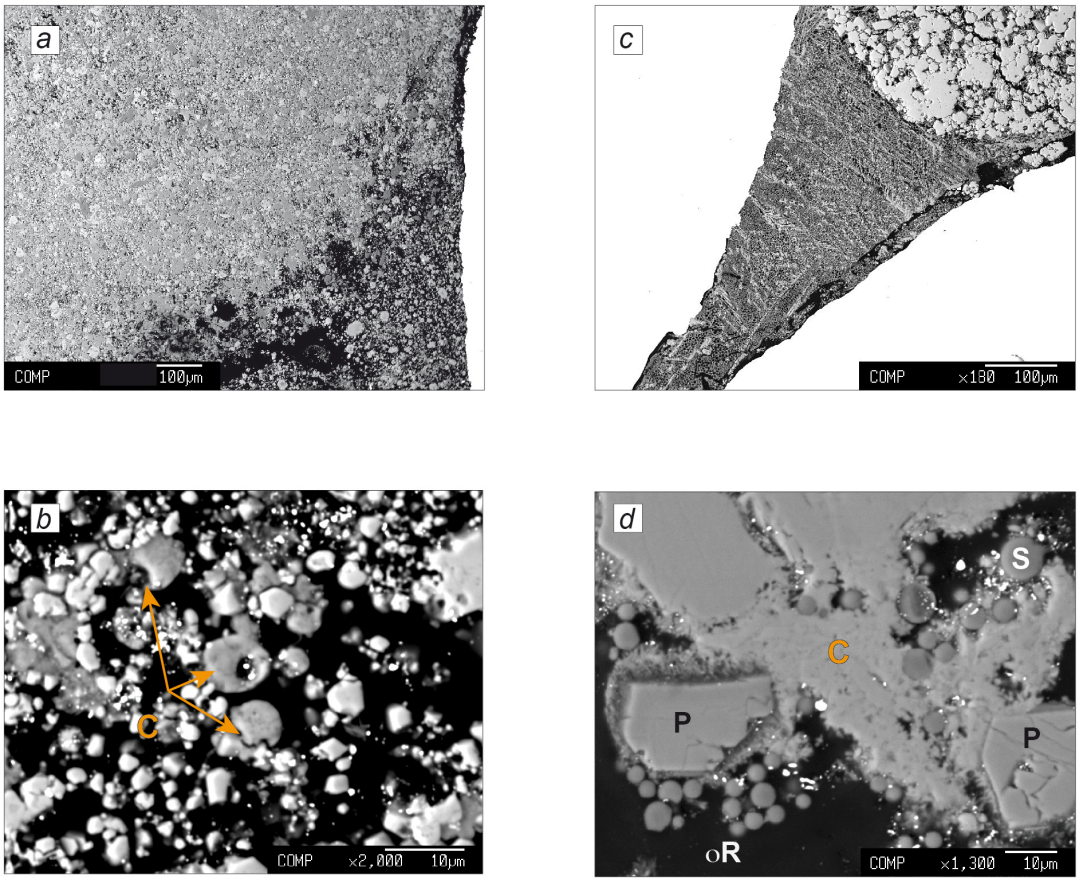
a
COMP 100µm
c
COMP ×180 100µm
b
C
COMP ×2,000 10µm
d
S
C
P
P
R
COMP ×1,300 10µm

Fig. S3

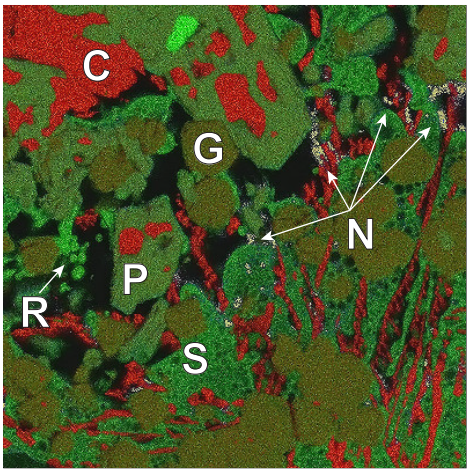

Fig. S4

Table S1. Bulk composition and CIPW norm of representative oceanic gabbros, and of starting material used in this study and in previous experimental studies.

	59-3	A1-2	593-ccb	OTB	SLEC1	SLEC3	OTBC	GA1cc	EC1
SiO_2	49.26	38.16	43.84	52.38	41.21	41.69	47.23	45.32	30.11
TiO_2	0.06	0.20	-	0.00	2.16	2.18	0.00	1.34	0.00
Al_2O_3	19.42	20.57	17.28	16.93	10.89	11.02	15.35	14.88	11.74
FeO	3.68	4.91	3.28	10.29	12.83	11.03	8.93	8.85	10.05
MnO	0.07	0.08	-	0.00	0.12	0.12	0.00	0.15	0.00
MgO	9.25	3.55	9.09	7.13	12.87	11.07	6.24	7.15	12.44
CaO	15.56	20.26	20.01	10.05	13.09	16.89	14.77	14.24	19.41
Na_2O	1.70	2.46	1.51	3.21	1.63	1.40	2.91	3.14	0.87
K_2O	0.01	0.09	0.01	0.00	0.11	0.10	0.02	0.40	0.00
CO_2	0.00	8.10	4.84	0.00	5.00	4.42	4.43	4.40	15.38
H_2O	0.00	0.96	0.38	0.00	0.00	0.00	0.12	0.50	0.00
Total	99.01	99.34	100.24	99.99	99.91	99.92	100.00	100.37	100.00
Mg/(Mg+Fe)	0.818	0.563	0.832	0.553	0.641	0.641	0.555	0.59	0.688
Ca/(Ca+Mg+Fe)	0.497	0.698	0.568	0.359	0.319	0.413	0.485	0.466	0.436
or	0.06	0.00	0.00	0.00	0.68	0.00	0.12	2.44	0.00
ab	15.11	0.00	0.00	28.67	5.04	0.00	17.20	10.61	0.00
an	44.87	49.00	41.51	31.62	23.14	24.61	29.99	26.21	32.53
lc	0.00	0.46	0.05	0.00	0.00	0.50	0.00	0.00	0.00
ne	0.00	14.49	8.37	0.00	6.18	7.90	6.02	11.10	5.42
di	25.23	17.12	37.42	14.38	35.95	46.74	37.12	39.40	0.00
hy	6.86	0.00	0.00	19.72	0.00	0.00	0.00	0.00	0.00
wo	0.00	0.00	0.00	0.00	0.00	0.00	0.00	0.00	0.00
ol	6.18	4.81	6.77	4.05	21.84	11.62	7.91	5.09	28.63
ac	0.00	0.00	0.00	0.00	0.00	0.00	0.00	0.00	0.00
mt	1.61	1.94	1.67	1.56	4.01	4.03	1.63	3.20	1.81
il	0.08	0.30	0.07	0.00	3.15	3.18	0.00	1.93	0.00
ap	0.00	0.46	0.00	0.00	0.00	0.00	0.00	0.00	0.00
wus	0.00	0.00	0.00	0.00	0.00	0.00	0.00	0.00	7.96

59-3: olivine gabbro from Southwest Indian Ridge[11]; A1-2: altered gabbro from Southwest Indian Ridge[12]; 59-3-ccb: bulk composition obtained from composition 59-3 by adding 11 wt% calcite and 1.24 wt% brucite; OTB: starting material used in ref. 14;

SLEC 1 and SLEC3: carbonated eclogite compositions[8]; OTBC: hydrated and carbonated material used in ref. 25; GA1cc: composition used in ref. 26; EC1: composition used in ref. 27.

Table S2. Summary of the starting material used, of experimental conditions, and of run products in order of abundance.

Run	Geometry	Bulk	P (GPa)	T (°C)	Duration (h)	H_2O (wt%)	CO_2 (wt%)	CO_2/H_2O (wt%)	carbonate st. mat. (wt%)	Volatile source	Run products
SPT1	Double-capsule	59-3	3.7	750	159	2.85	6.98	2.4	-	OAD	cpx + gar + law + mgs + dol + cs ± epi
SPT2	Double-capsule	59-3	3.8	775	146	2.85	6.98	2.4	-	OAD	cpx + gar + epi + dol + mgs + ky + cs
EFSP2	Double-capsule	59-3	3.8	800	110	2.85	6.98	2.4	-	OAD	cpx + gar + epi + dol + mgs + ky + cs
EFSP3	Double-capsule	59-3	3.8	900	92	2.85	6.98	2.4	-	OAD	cpx + gar + Mg-cc + glass + quench-cc + ky + cs
SPT3	Double-capsule	59-3	3.8	1000	121	2.85	6.98	2.4	-	OAD	cpx + gar + glass + Mg-cc + ky + cs
SPT7	Single-capsule	59-3-ccb	3.8	900	175	0.38	4.84	12.7	11	cc + br	cpx + gar + Mg-cc + epi + cs + quench-cc ± ky
FB6	Single-capsule	59-3-ccb	4.0	870	144	0.38	4.84	12.7	11	cc + br	cpx + gar + arg + quench-cc + ky + cs
SPT5	Single-capsule	59-3-ccb	4.2	900	105	0.38	4.84	12.7	11	cc + br	cpx + gar + arg + dol + quench-cc + glass + ky + cs
SPT6	Single-capsule	59-3-ccb	4.2	850	316	0.38	4.84	12.7	11	cc + br	cpx + gar + arg + ky + cs
SPT4	Single-capsule	59-3-ccb	4.6	700	264	0.38	4.84	12.7	11	cc + br	cpx + gar + law + dol + cs
SPT9	Sandwich	59-3-ccb-CA	4.2	850	86	3.7	10	2.7	26.7	$Al(OH)_3$ + cc + br	cpx + gar + arg + dol + ky + cs
SPT8	Sandwich	59-3-ccb-CA	4.2	900	234	3.7	10	2.7	26.7	$Al(OH)_3$ + cc + br	cpx + gar + quench-cc + glass + arg + Mg-cc + ky + cs
SPT10	Sandwich	59-3-ccb-CA	4.2	900	185	0.4	13.4	33.5	31	$Al(OH)_3$ + cc + br	cpx + gar + quench-cc + glass + arg + Mg-cc + ky + cs
SPT11	Sandwich	59-3-ccb-CA	4.2	900	201	1.3	13.4	10.3	31	$Al(OH)_3$ + cc + br	cpx + gar + quench-cc + glass + arg + Mg-cc + ky + cs

Geometry: double capsule indicates synthesis experiments performed at vapor-saturation, buffered at HM in the outer capsule; single capsule stands for experiments in single Au capsule, with an amount of volatiles adjusted to stabilize hydrous phases and carbonates only (see Methods); sandwich is for experiments in a single Au capsule, where a layer of carbonates is placed in between two layers of gels. H_2O, CO_2 and CO_2/H_2O are the total weight proportions and ratios of volatiles in the bulk composition. Carbonate st. mat. is the total amount of carbonate in the starting material, in weight proportions. Bulk: bulk composition of starting materials; 59-3 and 59-3-ccb: see Table S1; 59-3-ccb-CA: composition 59-3 with addition of a layer of Ca, Mg, Fe, Na carbonates, simulating the liquid produced at 4.2 GPa, 900 °C (see Table S3), and a layer of $Al(OH)_3$ + SiO_2, producing kyanite + H_2O at run conditions. Volatile sources: OAD: oxalic acid dihydrate; cc: calcite; br: brucite. Run products: arg: aragonite; cs: coesite; cpx: omphacite; dol: dolomite; epi: epidote; gar: garnet; glass: silicate glass; ky: kyanite; law: lawsonite; Mg-cc: (Mg,Fe)-calcite; mgs: magnesite; quench-cc: Ca-rich carbonate in dendritic, feathery or lobed/fingered morphology; it includes individual grains of Na-carbonate.

Table S3- Chemical composition of minerals and quench products in selected runs. Units are weight percent of oxides and atoms per formula unit. CIPW norm refer to silicate glass.

	clinopyroxene				garnet				epidote
Run	EFSP2	SPT3	SPT5	SPT8	EFSP2	SPT3	SPT5	SPT8	EFSP2
P(GPa)	3.8	3.8	4.2	4.2	3.8	3.8	4.2	4.2	3.8
T(°C)	800	1000	900	900	800	1000	900	900	800
SiO2	54.36 (1.15)	55.09 (1.17)	55.00 (0.42)	56.30 (0.44)	41.13 (1.35)	42.12 (0.29)	40.55 (0.09)	40.58 (0.42)	39.26 (0.19)
Al2O3	6.57 (1.02)	11.98 (1.15)	16.20 (0.59)	14.10 (0.45)	22.90 (0.45)	23.22 (0.38)	23.94 (0.38)	23.50 (0.18)	31.70 (0.18)
Fe2O3	0.00 (0.00)	0.00 (0.00)	0.00 (0.00)	0.00 (0.00)	0.00 (0.00)	0.33 (0.46)	0.41 (0.22)	0.38 (0.40)	1.26 (0.22)
FeO	2.09 (0.54)	1.89 (0.38)	1.81 (0.16)	1.78 (0.12)	10.72 (2.28)	7.98 (0.81)	10.47 (0.77)	10.99 (0.61)	0.00 (0.02)
MgO	13.59 (0.55)	11.08 (0.40)	8.29 (0.27)	8.10 (0.28)	12.49 (1.31)	14.49 (0.18)	8.57 (0.41)	8.42 (0.34)	0.46 (0.07)
CaO	21.26 (0.61)	17.17 (0.55)	13.90 (0.30)	13.70 (0.42)	12.21 (0.60)	12.61 (0.44)	17.47 (0.24)	16.92 (0.52)	24.03 (0.24)
Na2O	2.00 (0.11)	3.78 (0.30)	5.50 (0.22)	6.20 (0.38)	-	-	-	-	-
Total	99.88	100.98	100.70	100.18	99.45	100.75	101.41	100.79	96.71
Si	1.95 (0.02)	1.93 (0.02)	1.91 (0.01)	1.97 (0.01)	3.02 (0.05)	3.02 (0.02)	2.96 (0.01)	2.98 (0.03)	3.02 (0.01)
Al	0.28 (0.05)	0.49 (0.04)	0.67 (0.02)	0.58 (0.02)	1.98 (0.02)	1.96 (0.02)	2.06 (0.02)	2.04 (0.02)	2.87 (0.02)
Fe3	0.00 (0.00)	0.00 (0.00)	0.00 (0.00)	0.00 (0.00)	0.00 (0.00)	0.02 (0.02)	0.02 (0.01)	0.02 (0.02)	0.08 (0.01)
Fe2	0.06 (0.02)	0.06 (0.01)	0.05 (0.00)	0.05 (0.00)	0.66 (0.14)	0.48 (0.05)	0.64 (0.05)	0.68 (0.04)	0.00 (0.00)
Mg	0.73 (0.02)	0.58 (0.03)	0.43 (0.01)	0.42 (0.02)	1.37 (0.16)	1.55 (0.02)	0.93 (0.04)	0.92 (0.04)	0.05 (0.01)
Ca	0.82 (0.02)	0.64 (0.03)	0.52 (0.01)	0.51 (0.02)	0.96 (0.05)	0.97 (0.04)	1.37 (0.02)	1.33 (0.04)	1.98 (0.02)
Na	0.14 (0.01)	0.26 (0.02)	0.37 (0.01)	0.42 (0.03)	-	-	-	-	-

	magnesite	dolomite		(Mg,Fe)-calcite		quench carbonate			silicate glass
Run	EFSP2	SPT3	SPT8	SPT3	SPT8	SPT5	SPT8	Run	SPT8
P(GPa)	3.8	3.8	4.2	3.8	4.2	4.2	4.2	*P(GPa)*	4.2
T(°C)	800	800	900	1000	900	900	900	*T(°C)*	900
SiO2	-	-	-	-	-	1.79 (0.70)	1.79 (1.81)	SiO2	65.89 (3.32)
Al2O3	-	-	-	-	-	1.41 (0.18)	0.38 (0.21)	Al2O3	12.22 (1.68)
FeO	7.04 (3.15)	4.07 (0.73)	3.72 (0.39)	2.42 (0.41)	2.81 (0.29)	5.38 (0.39)	4.22 (0.43)	FeO	0.60 (0.77)
MgO	40.87 (2.97)	21.46 (10.47)	18.06 (1.67)	14.08 (0.36)	8.52 (0.43)	3.76 (0.26)	6.53 (0.35)	MgO	0.41 (0.04)
CaO	2.09 (0.79)	26.68 (9.16)	31.74 (0.69)	37.48 (0.74)	43.45 (1.55)	40.16 (0.85)	40.22 (1.43)	CaO	2.85 (0.65)
Na2O	0.06 (0.06)	0.09 (0.06)	0.04 (0.02)	0.07 (0.05)	0.06 (0.06)	2.26 (0.07)	2.27 (1.23)	Na2O	2.31 (1.90)
CO2	51.04 (0.74)	48.42 (4.66)	47.09 (1.71)	46.48 (0.70)	46.03 (0.95)	44.68 (0.43)	46.25 (1.08)		
Total	101.10	100.72	100.65	100.53	100.87	99.42	101.66	Total	84.28 (3.87)
Si	-	-	-	-	-	0.06 (0.02)	0.06 (0.06)	Q	51.38
Al	-	-	-	-	-	0.05 (0.01)	0.01 (0.01)	ab	25.19
Fe2	0.08 (0.04)	0.10 (0.02)	0.10 (0.01)	0.06 (0.01)	0.07 (0.01)	0.15 (0.01)	0.11 (0.01)	an	17.17
Mg	0.87 (0.05)	0.94 (0.37)	0.84 (0.05)	0.66 (0.01)	0.40 (0.02)	0.18 (0.01)	0.31 (0.02)	cor	4.28
Ca	0.03 (0.01)	0.89 (0.33)	1.06 (0.04)	1.27 (0.02)	1.48 (0.06)	1.41 (0.04)	1.36 (0.02)	hy	1.38
Na	0.00 (0.00)	0.01 (0.00)	0.00 (0.00)	0.00 (0.00)	0.00 (0.00)	0.14 (0.01)	0.14 (0.07)	mt	0.08
C	1.00 (0.00)	2.00 (0.00)	2.00 (0.00)	2.00 (0.00)	2.00 (0.00)	2.00 (0.00)	2.00 (0.00)	hem	0.52